

Manganese-doped indium oxide and its application in organic light-emitting diodes

Yaqin Liao, Qipeng Lu, Yi Fan, and Xingyuan Liu

Citation: *Appl. Phys. Lett.* **99**, 023302 (2011); doi: 10.1063/1.3610559

View online: <http://dx.doi.org/10.1063/1.3610559>

View Table of Contents: <http://apl.aip.org/resource/1/APPLAB/v99/i2>

Published by the [American Institute of Physics](#).

Related Articles

Novel exposure system using light-emitting diodes and an optical fiber array for printing serial numbers and code marks

Rev. Sci. Instrum. **83**, 045115 (2012)

Cavity suppression in nitride based superluminescent diodes

J. Appl. Phys. **111**, 083106 (2012)

Analytic model for the efficiency droop in semiconductors with asymmetric carrier-transport properties based on drift-induced reduction of injection efficiency

Appl. Phys. Lett. **100**, 161106 (2012)

Obvious efficiency enhancement of organic light-emitting diodes by parylene-N buffer layer

Appl. Phys. Lett. **100**, 163303 (2012)

Obvious efficiency enhancement of organic light-emitting diodes by parylene-N buffer layer

APL: Org. Electron. Photonics **5**, 93 (2012)

Additional information on *Appl. Phys. Lett.*

Journal Homepage: <http://apl.aip.org/>

Journal Information: http://apl.aip.org/about/about_the_journal

Top downloads: http://apl.aip.org/features/most_downloaded

Information for Authors: <http://apl.aip.org/authors>

ADVERTISEMENT

INSTRUMENTS FOR ADVANCED SCIENCE			
	Gas Analysis dynamic measurement of reaction gas streams catalysis and thermal analysis molecular beam studies dissolved species probes fermentation, environmental and ecological studies	Surface Science UHV TPD SIMS end point detection in ion beam etch elemental imaging - surface mapping	Plasma Diagnostics plasma source characterisation etch and deposition process reaction kinetic studies analysis of neutral and radical species
	Vacuum Analysis partial pressure measurement and control of process gases reactive sputter process control vacuum diagnostics vacuum coating process monitoring		
contact Hiden Analytical for further details: info@hiden.co.uk www.HidenAnalytical.com CLICK TO VIEW OUR PRODUCT CATALOGUE			

Manganese-doped indium oxide and its application in organic light-emitting diodes

Yaqin Liao,^{1,2} Qipeng Lu,¹ Yi Fan,¹ and Xingyuan Liu^{1,a)}

¹Key Laboratory of Excited State Processes, Changchun Institute of Optics, Fine Mechanics and Physics, Chinese Academy of Sciences, Changchun 130033, China

²Graduate School of Chinese Academy of Sciences, Beijing 100080, China

(Received 2 March 2011; accepted 22 June 2011; published online 12 July 2011)

Thin films of manganese-doped indium oxide (IMO) deposited by electron beam evaporation have been investigated as anodes in organic light-emitting diodes (OLEDs). The IMO films have a high work function of 5.35 eV, a desirable surface morphology with an average roughness of 1.1 nm, a high average optical transmittance of 87.2% in the visible region, and a maximum optical transmittance of 92% at 460 nm. It is demonstrated that an IMO anode can effectively improve hole injection at the anode/organic interface, resulting in OLEDs with an increased electroluminescent efficiency. © 2011 American Institute of Physics. [doi:10.1063/1.3610559]

Transparent conducting oxides (TCOs) are used extensively in optoelectronics applications such as photovoltaics and organic light-emitting diodes (OLEDs). Indium tin oxide (ITO) is the most widely used TCO anode in OLEDs and its properties have a significant influence on device performance.^{1–3} For example, the low work function (WF) of ITO causes imperfect energy alignment at the anode/organic interface with the highest occupied molecular orbital level of typical hole transporting layers (HTLs),⁴ which results in inefficient hole injection. Many reported TCOs including Al:ZnO (Ref. 5) and Zr:ZnO (Ref. 6) show favorable electrical conductivity and transparency. However, TCOs with a high WF and low surface roughness have seldom been reported.⁷ Manganese-doped indium oxides (IMOs) have been applied in spintronics,⁸ and gas⁹ and humidity sensors.¹ However, these IMOs exhibited high resistivity, which hampered their application in optoelectronics.¹⁰ In this work, films of IMO with improved electrical and optical properties that compare positively with those of ITO are produced. A hole injection contact can form effectively at the IMO/organic interface, resulting in green- and blue-emitting OLEDs with superior performance to the equivalent ITO-based devices.

An IMO film was deposited on a clean glass substrate by a technique involving two electron beam evaporation and End-Hall ion-assisted deposition (IAD) at a substrate temperature of 550 K. Electron beam deposition is relatively low in cost and more favorable for large area processing than pulsed laser deposition. IAD can be used to produce films that are smooth, microstructurally dense, and show improved adherence properties.¹¹ MnO and In₂O₃ powders of high purity were processed as two targets. The rates of evaporation and thickness of the films were monitored *in situ* by a thin film deposition controller. The rates of deposition of MnO and In₂O₃ were 0.2 and 2 Å/s, respectively. An IMO film with a thickness of 100 nm and sheet resistance (Rs) of 110 Ω/□ was deposited in a reactive oxygen atmosphere at a pressure of about 1.5×10^{-2} Pa. The Rs of the reference ITO film was 100 Ω/□. The carrier concentration, resistivity, and

carrier mobility of the IMO film were determined from Hall effect measurements. Transmittance spectra of the samples were measured by a Shimadzu UV-3101PC spectrophotometer (Japan). The components of the IMO film were analyzed by energy-dispersive X-ray spectroscopy (GENE SIS2000 XMS 60S). The WF of the samples was measured with a Kelvin probe (KP Technology, UK).

Typical green OLEDs containing ITO (device A), ITO/poly(3,4-ethylenedioxythiophene)–poly styrene sulfonic acid (PEDOT:PSS) (device B), IMO (device C), and IMO/PEDOT:PSS (device D) as anodes were fabricated to compare the effects of different anodes on device performance. The structure of the devices was as follows: glass/anode/4,4'-bis [N-(1-naphthyl)-N-phenylamino] biphenyl (NPB) (60 nm)/tris(8-hydroxyquinoline) (Alq₃) (60 nm)/LiF (0.5 nm)/Al (100 nm). To understand the hole injection characteristics of the IMO anode, hole-only devices containing different anodes with the structure glass/anode/NPB (100 nm)/Al (100 nm) were also fabricated. IMO and ITO surfaces were cleaned by immersion in a water bath in detergent for 30 min, washing with deionized water and subsequent ultrasonication in acetone for 15 min. The surface morphology of the different anodes was studied by atomic force microscopy (Veeco Dimension Icon, Veeco, USA). To demonstrate the general usage of IMO anodes in display devices, blue phosphorescent OLEDs (PHOLEDs) containing an IMO anode (device E) or reference ITO anode (device F) with the structure glass/anode/NPB (60 nm)/iridium(III) bis-[(4,6-difluorophenyl)-pyridinato-N,C²]picolate-doped N,N'-dicarbazolyl-3,5-benzene (7 wt. %, 30 nm)/2,9-dimethyl-4,7-diphenyl-1,10-phenanthroline (40 nm)/LiF (0.5 nm)/Al (100 nm) were fabricated. PEDOT:PSS films were prepared by spin-coating. The other organic layers and metal cathode were deposited sequentially by thermal evaporation under a vacuum of 4.0×10^{-4} Pa. The thickness of the films was measured with a surface profiler (Ambios XP-1, Ambios Technology, USA). The current-voltage characteristics were measured with a Keithley 2400 source meter (Keithley, USA). The luminance was recorded using a spectrophotometer (PR705, Photo Research, USA). All tests were performed under atmospheric conditions at room temperature.

^{a)} Author to whom correspondence should be addressed. Electronic mail: xingyuanliu@hotmail.com. Tel.: +86 431 86176341. Fax: +86 431 86176341.

TABLE I. Summary of the electrical and optical properties of IMO.

Mn composition (at. %)	Average transmittance (%)	Resistivity ($\Omega\text{-cm}$)	Mobility (cm^2/Vs)	Carrier concentration (cm^{-3})	Work function (eV)
2.68	87.2%	7.08×10^{-4}	43.4	2.033×10^{20}	5.35

The electrical and optical properties of an IMO film are presented in Table I and Fig. 1(a). Table I indicates that IMO is a potential n-type semiconductor because of its high electron concentration in the order of 10^{20} cm^{-3} and low resistivity of $7.08 \times 10^{-4} \Omega\text{-cm}$ with an electron mobility of $43.4 \text{ cm}^2/\text{V}\cdot\text{s}$. Fig. 1(a) shows the transmittance spectra of IMO and ITO films on glass substrates. In the visible region (380 to 780 nm), IMO has an average transmittance of 87.2%, which is slightly higher than that of the ITO reference (85.4%). The low transparency of ITO in the visible region is caused by its poor transmittance in the range from 380 to 500 nm. Fig. 1(a) shows that IMO has an average transmittance of nearly 90% in the blue range (from 400 to 500 nm),

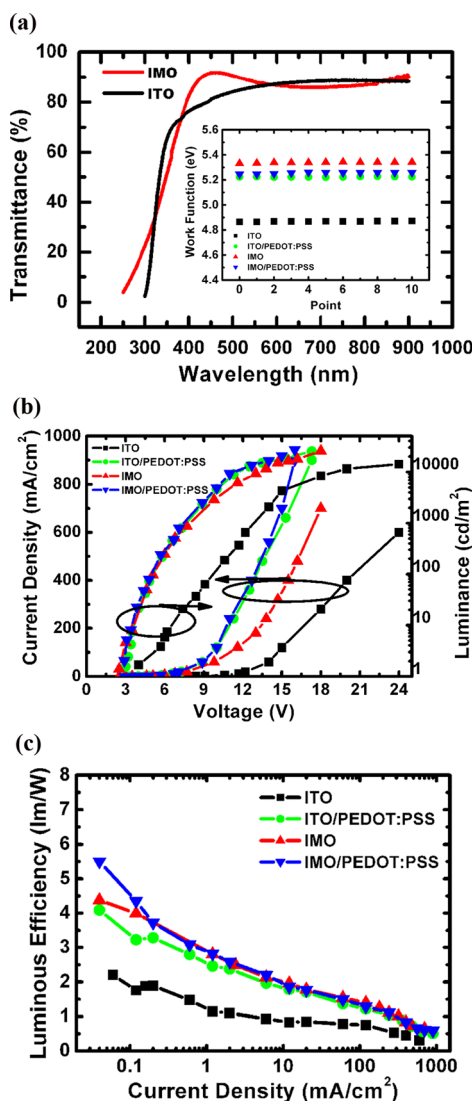


FIG. 1. (Color online) (a) Transmittance spectra of IMO and ITO. Inset: the WFs of various anodes. (b) J - V - L characteristics of devices A-D. (c) J - LE characteristics of devices A-D. Inset: energy level diagram of green OLEDs containing different anodes.

while that of ITO is less than 80%. In the green and red regions (from 500 to 780 nm), the average transmittances of IMO and ITO are 86.5 and 88%, respectively.

The WFs measured for IMO, ITO, IMO/PEDOT:PSS, and ITO/PEDOT:PSS anodes are illustrated in the inset of Fig. 1(a). IMO has a much higher WF (5.35 eV) than ITO (4.85 eV), ITO/PEDOT:PSS (5.22 eV), and IMO/PEDOT:PSS (5.25 eV). The nearly identical WFs of the PEDOT-modified ITO and IMO films are attributed to the thickness of the PEDOT:PSS film (30 nm).

Fig. 1(b) shows the current density-voltage-luminance (J - V - L) characteristics of devices containing different anodes. The presence of an IMO anode greatly improves device properties. At the same J , the operating voltage for neat IMO-based device C is significantly lower than that of neat ITO-based device A. The maximum L of device C (25690 cd/m^2 at 18 V) is 82% higher than that of device A (14120 cd/m^2 at 24 V). The carrier injection ability of the IMO (ITO) anode is enhanced by inserting a 30-nm-thick PEDOT:PSS layer between the IMO (ITO) anode and the HTL. Device B containing a PEDOT:PSS-modified ITO anode possess better J - V characteristics than that lacking a PEDOT:PSS layer (device C). Fig. 1(c) shows the current density-luminous efficiency (J - LE) characteristics of devices A-D. Device C has a significantly higher maximum LE (4.4 lm/W) than that of device A (2.2 lm/W), consistent with the J - V characteristics of these devices. Despite the fact that the J - V curve of device C is inferior to that of devices B and D, the trend of the J - LE curve of device C is slightly better than that of device B and almost identical to that of device D at high current density. This indicates that there is a favorable carrier balance in device C.

The differences in the performance of the devices could originate from their different hole injection abilities. The hole injection barrier between the anode and HTL and the surface roughness of the anode are the most important parameters influencing hole injection.^{2,3,7} As the WF of the anode increases, the energy barrier for hole injection decreases, leading to a lower voltage for injection to occur. Reducing the surface roughness of the anode will reduce the number of spikes on its surface and restrain the generation of defects. The effects of WF and surface roughness on the J - V characteristics of devices containing IMO anodes were studied using hole-only devices. The barrier height between IMO and NPB is only 0.05 eV. Furthermore, the average surface roughness of IMO (1.1 nm) is much lower than that of ITO (2.41 nm), as shown in Fig. 2(a). Therefore, the hole-only device containing an IMO anode shows significantly improved hole injection compared with the ITO-based hole-only device (Fig. 2(b)). The WF of IMO (5.35 eV) is higher than that of PEDOT:PSS-modified ITO (5.22 eV), but the hole injection ability of the IMO anode is still inferior to that of the PEDOT:PSS/ITO anode. This is because the PEDOT:PSS-modified ITO anode is smoother (average surface roughness of 0.84 nm) than the IMO anode. Fig. 2(a) shows that the spikes in the surface of the ITO anode are smoothed markedly by the addition of a PEDOT:PSS layer. Sharp spikes in the surface of an anode can cause breakdown and electrical shorting in OLEDs and seriously impede hole injection.^{2,3} The IMO/PEDOT:PSS anode possesses a superior hole injection

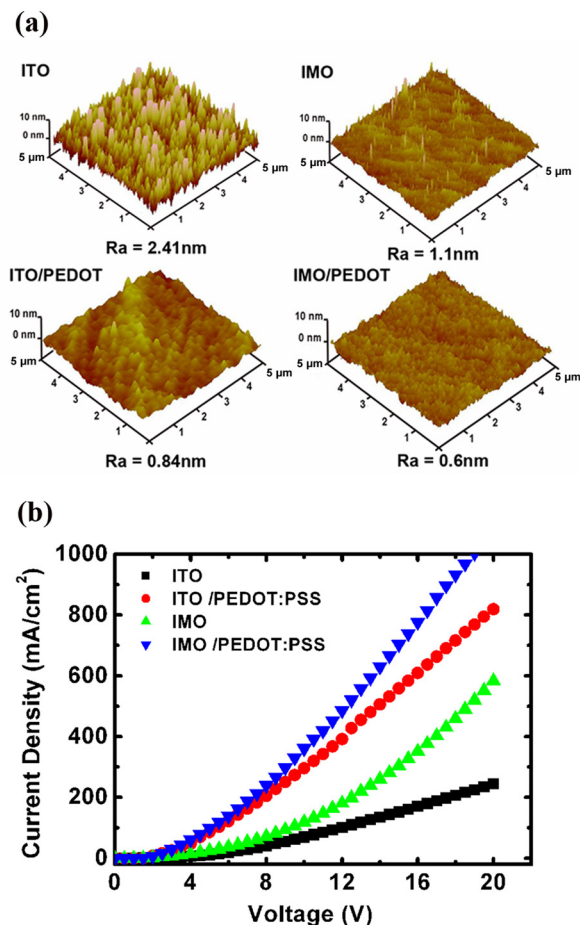


FIG. 2. (Color online) (a) Atomic force microscopy images of ITO, IMO, ITO/PEDOT:PSS, and IMO/PEDOT:PSS anodes. (b) J - V characteristics of hole-only devices containing different anodes.

ability to the ITO/PEDOT:PSS anode because of its smoother surface morphology (average roughness of 0.6 nm). The J - V characteristics of the hole-only devices containing different anodes indicate that the hole injection is enhanced when IMO is used as an anode in devices both with and without a PEDOT:PSS layer.

Fig. 3(a) shows the J - V - L characteristics of PHOLEDs containing IMO (device E) and ITO (device F) anodes. As anticipated, device E has significant improved J - V characteristics compared with those of device F because of the superior hole injection ability of the IMO anode. Device E possesses a low turn-on voltage of 3.7 V at a luminance of 2.8 cd/m², while that of device F is 4.7 V at a luminance of 1.9 cd/m². As shown in Fig. 3(b), the maximum LE of device E (17.8 lm/W) is enhanced by almost 87% compared with that of device F (9.5 lm/W). This can be mainly attributed to significantly improved hole injection from IMO to the HTL, and more effective light output in the blue region compared with the ITO-based device.

In summary, transparent conducting IMO anodes have been fabricated by a technique combining two electron beam evaporation and IAD. The IMO anode possesses a higher WF and lower surface roughness than those of commercial

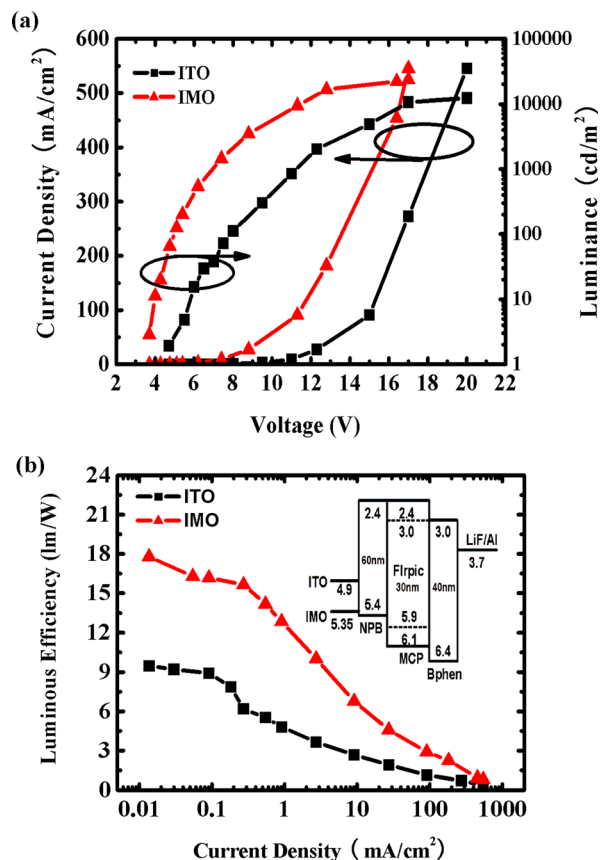


FIG. 3. (Color online) (a) J - V - L and (b) J - LE characteristics of PHOLED devices E and F. The inset shows the energy level diagram of these PHOLEDs.

ITO, which facilitate hole injection from the anode to the HTL. Both a typical green OLED and blue PHOLED containing an IMO anode show dramatically improved performance compared with reference devices containing ITO anodes.

This work was supported by the CAS Innovation Program, and the Jilin Province Science and Technology Research Project (Nos. 20090346 and 20100570).

- ¹C. C. Wu, C. I. Wu, and J. C. Sturm, *Appl. Phys. Lett.* **70**, 1348 (1997).
- ²Y. H. Tak, K. B. Kim, H. G. Park, K. H. Lee, and J. L. Lee, *Thin Solid Films* **411**, 12 (2002).
- ³G. Liu, J. B. Kerr, and S. Johnson, *Synth. Met.* **144**, 1 (2004).
- ⁴J. S. Kim, M. Granstrom, R. H. Friend, N. Johansson, W. R. Salaneck, R. Daik, W. J. Feast, and F. Cacialli, *J. Appl. Phys.* **84**, 6859 (1998).
- ⁵X. Jiang, F. L. Wong, M. K. Fung, and S. T. Lee, *Appl. Phys. Lett.* **83**, 1875 (2003).
- ⁶H. Kim, J. S. Horwitz, W. H. Kim, S. B. Qadri, and Z. H. Kafafi, *Appl. Phys. Lett.* **83**, 3809 (2003).
- ⁷N. Wang, X. X. Liu, and X. Y. Liu, *Adv. Mater.* **22**, 2211 (2010).
- ⁸D. Berardan, E. Guilmeau, and D. Pelloquin, *J. Magn. Magn. Mater.* **320**, 983 (2008).
- ⁹G. Korotcenkov, I. Boris, V. Brinzari, V. Golovanov, Y. Lychkovsky, G. Karkotsky, A. Cornet, E. Rossinyol, J. Rodrigue, and A. Cirera, *Sens. Actuators B* **103**, 13 (2004).
- ¹⁰R. B. H. Tahir, T. Ban, Y. Ohya, and Y. Takahashi, *J. Am. Ceram. Soc.* **81**, 321 (1998).
- ¹¹Y. Yang, Q. L. Huang, A. W. Metz, J. Ni, S. Jin, T. J. Marks, M. E. Madsen, A. DiVenere, and S. T. Ho, *Adv. Mater.* **16**, 321 (2004).